Vibration isolation effect study of in-filled trench barriers to train-induced environmental vibrations

Soil Dynamics and Earthquake Engineering 125 (2019) 105741

Contents lists available at ScienceDirect

Soil Dynamics and Earthquake Engineering

journal homepage: www.elsevier.com/locate/soildyn

Vibration isolation effect study of in-filled trench barriers to train-induced environmental vibrations

Jinbao Yao[a,b,*], Rutao Zhao[a], Nan Zhang[a], Dujuan Yang[b]

[a] School of Civil Engineering, Beijing Jiaotong University, Beijing, 100044, China
[b] Information Systems in the Built Environment Group, Eindhoven University of Technology, PO Box 513, Den Dolech 2, 5600 MB, Eindhoven, the Netherlands

ARTICLE INFO

Keywords:
Isolation
Infilled trench
Train
Rayleigh wave
Environmental vibration

ABSTRACT

An in-filled trench barrier is usually used to reduce the damages from train-induced environmental vibrations. To find the vibration isolation effect of an in-filled trench barrier, this paper analyses the reflection coefficients and transmission coefficients of the Rayleigh wave at the interface between in-filled trenches and the soil. In our calculation formulas of ground vibrations, a single point and a single frequency excitation, as well as multi-point and multi-frequency excitation, are simultaneously derived in a soil-in-filled-trench system.

Using these formulas and a numerical analysis, the effects of an in-filled trench barrier on the environmental vibrations induced by running trains are analyzed. The results show that the reflection coefficients increase, while the transmission coefficients decrease, with the density and elastic modulus of the in-filled material. The vibration isolation effect is clearly better than that without trenches. In a certain width range, the transmission coefficient and vertical acceleration levels decrease with the increase of trench width. The influences of the transmission coefficient and the vibration isolation effects are not clear with the trenches' depth variation. The vertical vibrations of the ground pick-up point are all smaller than those without in-filled trenches.

1. Introduction

With the development of social economy and increases of standards of living, the problem of environment vibrations has become greater. Traffic-induced vibrations can propagate through nearby soil, inducing secondary vibrations and noises of nearby buildings, which have considerable effect on structural safety, as well as the routine life and work of residents living in buildings along traffic-lines. Vibration damages induced by running trains have become one of the seven public pollution, which has garnered greater attention from engineers and researchers in China and abroad [1–3]. To reduce vibration damages, many scholars have carried out many studies on environmental vibration isolation induced by railway traffic. In these studies, many researchers focused on the ground surface vibration problems with barrier vibration isolation [4–6]. When an elastic wave encounters an in-filled trench barrier, because of the discontinuity between two different mediums, the reflected and transmitted waves appeared at the interface between the barrier and the soils. Simultaneously, the energy of soil vibration will be reduced after the wave passes through the barriers; therefore, the effect of vibration isolation can be examined.

The essence of barrier vibration isolation is the propagation of elastic waves in a non-homogeneous medium. Elastic waves will produce different reflected waves and transmitted waves under different medium parameters. The laws of reflection and transmission changes at the discontinuous medium surface are very important for studies of vibration isolation theory. Wood [7] defines the barrier vibration isolation performance indicators in the literature. Beskos et al. [8] discussed the steady-state and transient vibration isolation of in-filled trenches with the boundary element method coupled Fourier transform. Yang et al. [9] studied two-dimensional vibration isolation of in-filled trenches using finite element and boundary element coupling methods. Yang et al. [10] studied the propagation characteristics of plane shear-wave (SH wave) and primary wave (P wave) through the elastic inter-layer and derived the SH wave and P wave. The relationship between the transmission and reflection coefficients at the discontinuous dielectric surface with the different media parameters and incidence angles was defined. Andersen et al. [11] deduced the thin-layer element boundaries for a 2.5- dimensional finite element. Other methods against train-induced vibrations can be found in these literatures [12,13].

In the vibration isolation studies of in-filled trench barriers, Lysmer and Waas [14] studied the vibration isolation effect of clay mud material-filled trenches using the concentrated mass method. Ahmad and Al-Hussaini et al. [15] used the boundary element method to analyse

* Corresponding author. School of Civil Engineering, Beijing Jiaotong University, Beijing, 100044, China.
E-mail address: jbyao@bjtu.edu.cn (J. Yao).

https://doi.org/10.1016/j.soildyn.2019.105741
Received 8 January 2019; Received in revised form 29 May 2019; Accepted 24 June 2019
Available online 08 July 2019
0267-7261/

the passive vibration isolation effects of in-filled trenches. Bose et al. [16] used a 3D finite element method to analyse the Efficiency of Open and Infill Trenches in Mitigating Ground-Borne Vibrations. Zoccali et al. [17] introduced infilled trenches mitigation capacity and length influence against bound-vibrations induced by trains. Garinei et al. [18] analyzed the efficiency of trenches for the mitigation of train-induced vibrations by some experimental evaluation.

In the propagation of vibration waves in the soil, the Rayleigh wave attenuation gradients are considerably smaller than that of the body wave. Studies have shown that Rayleigh waves can account for 67% of the environmental vibration components [19]. Therefore, it is more practical to study the attenuation laws of barrier vibration isolation and their effect on Rayleigh waves. However, in the past, many studies have used the numerical analysis and experimental research methods. In this paper, the propagation characteristics of the Rayleigh waves passing through in-filled trench barriers are studied by a theoretical analysis method. The reflection coefficient and transmission coefficient of Rayleigh waves at the interface between the in-filled trench and the soil are deduced; furthermore, the calculation formulas of the vibration response of the ground surface pick-up point caused by different types of excitation are derived. The effects of in-filled trench barrier on the environmental vibration caused by trains are analyzed.

2. Effect of in-filled trench on Rayleigh wave propagation

2.1. Rayleigh wave propagation

Vibrations on the ground surface induced by a running train often spread long distances through Rayleigh waves. Rayleigh wave propagation has two directions, The displacements in the vertical direction z and the horizontal direction x are related to the wave function φ and ψ of the Rayleigh wave. The wave functions of the Rayleigh wave can be defined as

$$\begin{cases} \varphi = \mathrm{A}e^{-rz}e^{i(\omega t - k_\gamma x)} \\ \psi = Be^{-sz}e^{i(\omega t - k_\gamma x)} \end{cases} \tag{1}$$

where A and B are constants; $k_\gamma = \omega/\gamma$, γ represents the Rayleigh wave velocity, and ω is the fluctuation circle.

Frequency. The displacements of Rayleigh waves along the vertical and horizontal directions can be expressed by the wave functions φ andψ, respectively, as

$$u = \frac{\partial \varphi}{\partial x} - \frac{\partial \psi}{\partial z},\ w = \frac{\partial \varphi}{\partial z} + \frac{\partial \psi}{\partial x} \tag{2}$$

where u and w represent the vertical and horizontal displacements, respectively.

Under the action of concentrated harmonic load $f(t) = Pe^{i\omega t}$, where P is the amplitude and ω is the circular frequency of load, the horizontal displacement u and the vertical displacement w of the Rayleigh wave from the load distance r can be expressed as

$$\begin{cases} u \approx \frac{P}{\mu r}\bar{\xi}\sqrt{\frac{\hat{k}\bar{r}}{2\pi}}e^{-i\left(\hat{k}\bar{r}+\pi/4\right)}e^{i\omega t} \\ w \approx \frac{P}{\mu r}\chi\sqrt{\frac{\hat{k}\bar{r}}{2\pi}}e^{-i\left(\hat{k}\bar{r}+3\pi/4\right)}e^{i\omega t} \end{cases} \tag{3}$$

where μ is the Ram constant $\bar{r}$ and $\hat{k}$ are the dimensionless frequency and stiffness, respectively; $\bar{\xi}$ and χ are the vertical and horizontal attenuation coefficients in the Rayleigh wave propagation process, respectively.

2.2. Reflection and transmission of the Rayleigh waves at different media

De Bremaecker [20] and Lapwood [21] studied the reflection and transmission of Rayleigh waves at an angle by experimental methods and proposed the influence of the angle on the reflection and transmission of Rayleigh waves. It is believed that in the quarter space, at the interface of two solid elastic media, the two sides of the interface are in close contact, and the boundary conditions require that the stress and displacement of two sides are continuous, that is, the respective stress difference and displacement difference on both sides of the contact surface equal zero, or the residual is equal to zero, as shown in Fig. 1. φ1, φ2, φ3 and Ψ1, Ψ2, Ψ3 are the wave potential functions of incident wave, reflected wave and transmitted wave in two different medias, respectively.

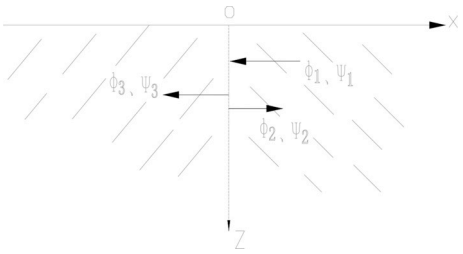

Fig. 1. Schematic diagram of Rayleigh wave propagation in a discontinuous surface of a 1/4 space medium.

The Rayleigh waves have complex waveform conversion on the medium surface. In general, the reflection and transmission of Rayleigh waves are unable to meet the boundary conditions with zero residual on both sides of contact surface, but by selecting the appropriate reflection coefficient R and transmission T, its residual reaches the minimum in the sense of least squares. That is, by selecting the appropriate reflection coefficient $R = A_2/A_1$ and the transmission coefficient $T = A_3/A_1$, (A_1, A_2, and A_3 are the amplitudes of the incident waves, reflected waves and transmitted Rayleigh waves, respectively); therefore, the integral formula 4 obtains the minimum value.

$$\begin{aligned} I_o = &\frac{1}{I_1}\int_0^\infty \{|\sigma_{xx} - \sigma_{xx}'|^2 + |\tau_{xz} - \tau_{xz}'|^2\}dz \\ &+ \frac{1}{I_2}\int_0^\infty \{|u - u'|^2 + |w - w'|^2\}dz \end{aligned} \tag{4}$$

where I_1 and I_2 are the integral expressions of stress and displacement generated by the Rayleigh waves at the discontinuous plane of the medium, respectively, and can be calculated by formula 5. σ_{xx}, σ_{xx}', τ_{xz}, τ_{xz}', u, u',w, w' are the normal stresses, shear stresses, vertical displacements and horizontal displacements in the two different medias, respectively.

$$\begin{cases} I_1 = \int_0^\infty \{|\sigma_{xxo}|^2 + |\tau_{xzo}|^2\}dz \\ I_2 = \int_0^\infty \{|u_0|^2 + |w_0|^2\}dz \end{cases} \tag{5}$$

where σ_{xxo}, τ_{xzo}, u_o, w_o are the normal stresses, shear stresses, vertical displacements and horizontal displacements at the interface position, respectively. By calculation and simplification, the expression of I_0 can be obtained as

$$\begin{aligned} I_o = &(A + J)(1 + R)^2 + (B + G)(1 - R)^2 + (C + E + H + K)T^2 \\ &+ (D + L)T(1 + R) + (F + I)T(1 - R) \end{aligned} \tag{6}$$

where A to L are functions only related to the two medium parameters, which can be obtained by calculations derived later. To make I_0 reach the minimum, let $\frac{\partial I_0}{\partial R} = \frac{\partial I_0}{\partial T} = 0$; therefore, the reflection coefficient R and the transmission coefficient T can be obtained.

2.2. Rayleigh waves along the in-filled trench propagation path

When the Rayleigh waves encounter the in-filled trenches, the incident Rayleigh waves can be converted into the following three kinds of waves: the first is the reflective Rayleigh wave, the second is the radiated transmission Rayleigh wave, the third is the body wave

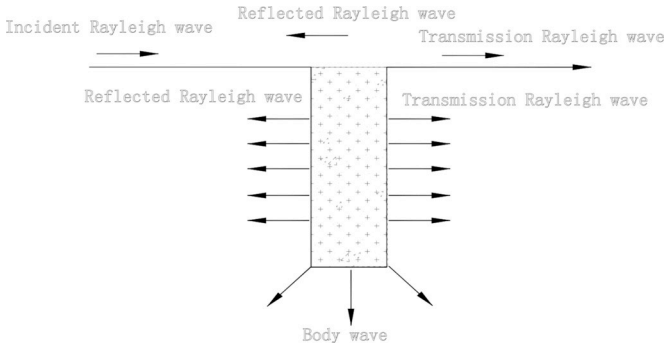

Fig. 2. Schematic diagram of the propagation of incident Rayleigh waves at the in-filled trenches.

radiating outward at the surface of the medium, as shown in Fig. 2.

Li et al. [22] studied the reflection and transmission of the Rayleigh waves at the interfaces of different media. When Rayleigh waves are incident on the discontinuous medium, they are mainly propagated in the horizontal direction. The wave energy propagating downward and upward along the vertical interface is very small, which may not be considered when deriving the reflection coefficient and transmission coefficient of the Rayleigh waves.

Gao et al. [28] found that the in-filled trench barrier depth has little effect on the vibration isolation effect when the barrier depth is greater than twice the Rayleigh wave wavelength. In this paper, in-filled trench materials can also be regarded as an elastic inter layer. Therefore, the propagation and attenuation problems of the Rayleigh waves through the in-filled trenches can be converted to the reflection and transmission problems of the Rayleigh waves through the elastic inter-layer. Then, the following assumptions can be made:

First, when the Rayleigh wave passes through the elastic inter-layer, reflection and transmission occur only in the discontinuous faces of two medias.

Second, the steady-state waves in the elastic inter-layer are represented by a single left-going wave and a single right-travelling wave.

3. Reflection and transmission coefficients of Rayleigh waves through in-filled trenches

According to the description in section 2, when the vibration wave encounters in-filled trench barriers during the propagation process, two reflections and transmissions will occur at the contact surface between the soil and the in-filled trenches. As shown in Fig. 3, φ1, φ2, φ3, φ4, φ5 and Ψ1, Ψ2, Ψ3, Ψ4, Ψ5 are the wave potential functions of incident wave, reflected wave and transmitted wave in two different medias, respectively. The distance between the excitation force and the left edge of in-filled trenches is L_P, and the trench width is d. If the reflection and transmission coefficients at the contact surface of the in-filled trench can be derived, the displacement and stress analytical expressions of the surface pick-up points can be obtained.

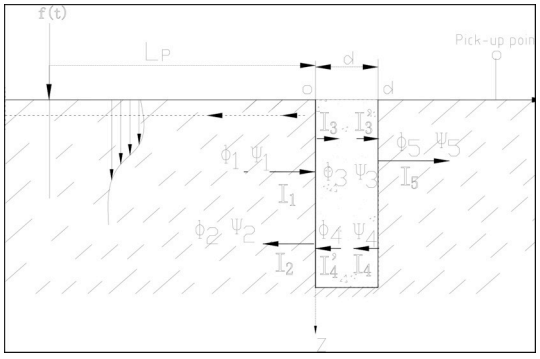

Fig. 3. Schematic diagram of reflection and transmission at the in-filled trench.

3.1. Reflection and transmission coefficient derivation

As shown in Fig. 3, when the incident wave I_1 is of normal incidence to the interface (x = 0) between the in-filled trench and the soil, the reflected Rayleigh wave I_2 is generated. At the same time, the transmitted Rayleigh waves I_3 will produce reflection and transmission at the other interface (x = d), so the right-line transmission Rayleigh waves I_5 and the left-line reflection Rayleigh waves I_4 will be generated at the interface (x = d). Formula 7 shows that different Rayleigh waves can be expressed by the wave potential function.

$$\begin{cases} \varphi_1 = A_1 e^{-rz} e^{i(\omega t - k_\gamma x)},\ \psi_1 = B_1 e^{-sz} e^{i(\omega t - k_\gamma x)} \\ \varphi_2 = A_2 e^{-rz} e^{i(\omega t + k_\gamma x)},\ \psi_2 = B_2 e^{-sz} e^{i(\omega t + k_\gamma x)} \\ \varphi_3 = A_3 e^{-r'z} e^{i(\omega t - k'_\gamma x)},\ \psi_3 = B_3 e^{-s'z} e^{i(\omega t - k'^{\gamma} x)} \\ \varphi_4 = A_4 e^{-r'z} e^{i(\omega t + k'_\gamma x)},\ \psi_4 = B_4 e^{-s'z} e^{i(\omega t + k'_\gamma x)} \\ \varphi_5 = A_5 e^{-rz} e^{i(\omega t - k_\gamma x)},\ \psi_5 = B_5 e^{-sz} e^{i(\omega t - k_\gamma x)} \end{cases} \tag{7}$$

For the right-line wave, the Rayleigh wave characteristic equations are as follows:

$$\begin{cases} \mu(2k_\gamma^2 - k_\beta^2)A_i + 2\mu i k_\gamma s B_i = 0 \\ \mu[2ik_\gamma r A_i - (2k_\gamma^2 - k_\beta^2)B_i] = 0 \end{cases} \tag{8}$$

3.2. Rayleigh wave reflection and transmission analysis at the interface of $x = d$

On the left side of x = d, the stress and the displacement can be expressed as

$$\begin{cases} \sigma_{xx} = \lambda'\left(\frac{\partial^2\varphi}{\partial x^2} + \frac{\partial^2\varphi}{\partial z^2}\right) + 2\mu'\left(\frac{\partial^2\varphi}{\partial x^2} - \frac{\partial^2\psi}{\partial z \partial x}\right) = (-\mu' a' e^{-r'z} + \mu' b' e^{-s'z})(A_3 \\ \qquad e^{i(\omega t - k'^{\gamma} x)} + A_4 e^{i(\omega t + k'^{\gamma} x)}) \\ \tau_{xz} = \mu'\left(2\frac{\partial^2\varphi}{\partial x \partial z} + \frac{\partial^2\psi}{\partial x^2} - \frac{\partial^2\psi}{\partial z^2}\right) = 2\mu' i r' k'_\gamma \cdot (e^{-r'z} - e^{-s'z}) \cdot (A_3 \\ \qquad e^{i(\omega t - k'^{\gamma} x)} - A_4 e^{i(\omega t + k'^{\gamma} x)}) \\ u = ik'_\gamma \cdot \left(\frac{2s'r'}{b'} e^{-s'z} - e^{-r'z}\right) \cdot (A_3 e^{i(\omega t - k'^{\gamma} x)} - A_4 e^{i(\omega t + k'^{\gamma} x)}) \\ w = -r' \cdot \left(e^{-r'z} - \frac{2k'^2_\gamma}{b'} e^{-s'z}\right) \cdot (A_3 e^{i(\omega t - k'^{\gamma} x)} + A_4 e^{i(\omega t + k'^{\gamma} x)}) \end{cases} \tag{9}$$

On the right side of x = d, the stress and the displacement can be expressed as

$$\begin{cases} \sigma'_{xx} = -\mu(ae^{-rz} - be^{-sz}) A_5 e^{i(\omega t - k_\gamma x)} \\ \tau'_{xz} = 2\mu i r k_\gamma \cdot (e^{-rz} - e^{-sz}) \cdot A_5 e^{i(\omega t - k_\gamma x)} \\ u' = ik_\gamma \cdot \left(\frac{2sr}{b} e^{-sz} - e^{-rz}\right) \cdot A_5 e^{i(\omega t - k_\gamma x)} \\ w' = -r \cdot \left(e^{-rz} - \frac{2k_\gamma^2}{b} e^{-sz}\right) \cdot A_5 e^{i(\omega t - k_\gamma x)} \end{cases} \tag{10}$$

The stress and the displacement expressions caused by incident waves I_3 are

$$\begin{cases} \sigma_{xxo} = -\mu'(a' e^{-r'z} - b' e^{-s'z}) A_3 e^{i(\omega t - k'^{\gamma} x)} \\ \tau_{xzo} = 2\mu' i r' k'_\gamma \cdot (e^{-r'z} - e^{-s'z}) A_3 e^{i(\omega t - k'^{\gamma} x)} \\ u_o = ik'_\gamma \cdot \left(\frac{2s'r'}{b'} e^{-s'z} - e^{-r'z}\right) \cdot A_3 e^{i(\omega t - k'^{\gamma} x)} \\ w_o = -r' \cdot \left(e^{-r'z} - \frac{2k'^2_\gamma}{b'} e^{-s'z}\right) \cdot A_3 e^{i(\omega t - k'^{\gamma} x)} \end{cases} \tag{11}$$

The residual I_0 on the both sides of x = d can be expressed as

$$I_o = \frac{1}{I_1}\int_0^l \{|\sigma_{xx} - \sigma_{xx}'|^2 + |\tau_{xz} - \tau_{xz}'|^2\}dz + \frac{1}{I_2}\int_0^l \{|u - u'|^2 + |w - w'|^2\}dz \tag{12}$$

In Equation (12), by omitting the common phase e^{iwt} in part of each functional formula, I_1 and I_2 can be respectively obtained as

$$\begin{cases} I_1 = \int_0^l \{|\sigma_{xxo}|^2 + |\tau_{xzo}|^2\}dz = \mu'^2 A_3^2 \cdot \left[\left(a'^2 + \frac{b'^2 r'}{s'}\right) \cdot \frac{1 - e^{-2r'l}}{2r'} + \left(b'^2 + \frac{b'^2 r'}{s'}\right) \cdot \frac{1 - e^{-2s'l}}{2s'} - \left(2a'b' + \frac{2b'^2 r'}{s'}\right) \cdot \frac{1 - e^{-(r'+s')l}}{r' + s'} \right] \\ I_2 = \int_0^l \{|u_o|^2 + |w_o|^2\}dz = A_3^2 \cdot \left[(k'^2_\gamma + r'^2) \cdot \frac{1 - e^{-2r'l}}{2r'} + \frac{b'r'}{s'} \cdot \frac{1 - e^{-2s'l}}{2s'} - \frac{b'(s' + r')}{s'} \cdot \frac{1 - e^{-(r'+s')l}}{r' + s'} \right] \end{cases} \tag{13}$$

At the interface of x = d, the reflection coefficient R' and the transmission coefficient T' can be expressed as follows: $R' = A_4/A_3$, $T' = A_5/A_3$. Bring Equation (11) and Equation (10) into Equation (9), the integral I_0 can be expressed by the parameter R' and the parameter T'. After calculation, the constant A, B,.., I, J, K, L can be expressed as.

$$A = \frac{1}{2\alpha'_0}\left[\left(a'^2 + \frac{b'^2 r'}{s'}\right) \frac{1 - e^{-2r'l}}{2r'} + \left(b'^2 + \frac{b'^2 r'}{s'}\right) \frac{1 - e^{-2s'l}}{2s'} - \left(2a'b' + \frac{2b'^2 r'}{s'}\right) \frac{1 - e^{-(r'+s')l}}{r' + s'} \right] + \frac{\cos(2k'_\gamma d)}{2\alpha'_0}\left[\left(a'^2 - \frac{b'^2 r'}{s'}\right) \frac{1 - e^{-2r'l}}{2r'} + \left(b'^2 - \frac{b'^2 r'}{s'}\right) \frac{1 - e^{-2s'l}}{2s'} - \left(2a'b' - \frac{2b'^2 r'}{s'}\right) \frac{1 - e^{-(r'+s')l}}{r' + s'} \right] \tag{14}$$

$$B = \frac{1}{2\alpha'_0}\left[\left(a'^2 + \frac{b'^2 r'}{s'}\right) \frac{1 - e^{-2r'l}}{2r'} + \left(b'^2 + \frac{b'^2 r'}{s'}\right) \frac{1 - e^{-2s'l}}{2s'} - \left(2a'b' + \frac{2b'^2 r'}{s'}\right) \frac{1 - e^{-(r'+s')l}}{r' + s'} \right] - \frac{\cos(2k'_\gamma d)}{2\alpha'_0}\left[\left(a'^2 - \frac{b'^2 r'}{s'}\right) \frac{1 - e^{-2r'l}}{2r'} + \left(b'^2 - \frac{b'^2 r'}{s'}\right) \frac{1 - e^{-2s'l}}{2s'} - \left(2a'b' - \frac{2b'^2 r'}{s'}\right) \frac{1 - e^{-(r'+s')l}}{r' + s'} \right]$$

$$C = \frac{1}{\alpha'_0}\left(\frac{\mu}{\mu'}\right)^2 \left(a^2 \cdot \frac{1 - e^{-2rl}}{2r} + b^2 \cdot \frac{1 - e^{-2sl}}{2s} - 2ab \cdot \frac{1 - e^{-(r+s)l}}{r + s} \right)$$

$$D = -\frac{1}{\alpha'_0}\left(\frac{\mu}{\mu'}\right) \cdot \cos(k'_\gamma d - k_\gamma d) \cdot \left[(2a'a + 8k'_\gamma k_\gamma r'r) \cdot \frac{1 - e^{-(r+r')l}}{r + r'} + (2bb' + 8k'_\gamma k_\gamma r'r) \cdot \frac{1 - e^{-(s+s')l}}{s + s'} \right] + \frac{1}{\alpha'_0}\left(\frac{\mu}{\mu'}\right) \cdot \cos(k'_\gamma d - k_\gamma d) \cdot \left[(2a'b + 8k'_\gamma k_\gamma r'r) \cdot \frac{1 - e^{-(r'+s)l}}{r' + s} + (2ab' + 8k'_\gamma k_\gamma r'r) \cdot \frac{1 - e^{-(r+s')l}}{r + s'} \right]$$

$$E = \frac{1}{\alpha'_0}\left(\frac{\mu}{\mu'}\right)^2 \frac{b^2 r}{s}\left(\frac{1 - e^{-2rl}}{2r} + \frac{1 - e^{-2sl}}{2s} - 2 \cdot \frac{1 - e^{-(r+s)l}}{r + s} \right)$$

$$F = \frac{1}{\alpha'_0}\left(\frac{\mu}{\mu'}\right) \cdot \cos(k'_\gamma d + k_\gamma d) \cdot \left[(-2a'a + 8k'_\gamma k_\gamma r'r) \cdot \frac{1 - e^{-(r+r')l}}{r + r'} + (-2bb' + 8k'_\gamma k_\gamma r'r) \cdot \frac{1 - e^{-(s+s')l}}{s + s'} \right] - \frac{1}{\alpha'_0}\left(\frac{\mu}{\mu'}\right) \cdot \cos(k'_\gamma d + k_\gamma d) \cdot \left[(-2a'b + 8k'_\gamma k_\gamma r'r) \cdot \frac{1 - e^{-(r'+s)l}}{r' + s} + (-2ab' + 8k'_\gamma k_\gamma r'r) \cdot \frac{1 - e^{-(r+s')l}}{r + s'} \right]$$

$$G = \frac{1}{2\beta'_0}\left[(k'^2_\gamma + r'^2) \frac{1 - e^{-2r'l}}{2r'} + \frac{b'r'}{s'} \cdot \frac{1 - e^{-2s'l}}{2s'} - \left(b' + \frac{b'r'}{s'}\right) \frac{1 - e^{-(r'+s')l}}{r' + s'} \right] + \frac{\cos(2k'_\gamma d)}{2\beta'_0}\left[(k'^2_\gamma - r'^2) \frac{1 - e^{-2r'l}}{2r'} - \frac{k'^2_\beta r'}{s'} \cdot \frac{1 - e^{-2s'l}}{2s'} - \left(b' - \frac{b'r'}{s'}\right) \frac{1 - e^{-(r'+s')l}}{r' + s'} \right]$$

$$H = \frac{1}{\beta'_0}\left(k^2_\gamma \cdot \frac{1 - e^{-2rl}}{2r} + sr \cdot \frac{1 - e^{-2sl}}{2s} - b \cdot \frac{1 - e^{-(r+s)l}}{r + s} \right)$$

$$I = \frac{1}{\beta'_0} \cdot 2\cos(k'_\gamma d + k_\gamma d) \cdot \left[(k'_\gamma k_\gamma - r'r) \cdot \frac{1 - e^{-(r+r')l}}{r + r'} + \left(\frac{4k'_\gamma k_\gamma s'sr'r}{bb'} - \frac{4k'^2_\gamma k^2_\gamma r'r}{bb'} \right) \cdot \frac{1 - e^{-(s+s')l}}{s + s'} \right] - \frac{1}{\beta'_0} \cdot 2\cos(k'_\gamma d + k_\gamma d) \cdot \left[\left(\frac{2srk'_\gamma k_\gamma}{b} - \frac{2k^2_\gamma r'r}{b} \right) \cdot \frac{1 - e^{-(r'+s)l}}{r' + s} + \left(\frac{2s'r'k'_\gamma k_\gamma}{b'} - \frac{2k'^2_\gamma r'r}{b'} \right) \cdot \frac{1 - e^{-(r+s')l}}{r + s'} \right]$$

$$J = \frac{1}{2\beta'_0}\left[(k'^2_\gamma + r'^2) \frac{1 - e^{-2r'l}}{2r'} + \frac{b'r'}{s'} \cdot \frac{1 - e^{-2s'l}}{2s'} - \left(b' + \frac{b'r'}{s'}\right) \frac{1 - e^{-(r'+s')l}}{r' + s'} \right] - \frac{\cos(2k'_\gamma d)}{2\beta'_0}\left[(k'^2_\gamma - r'^2) \frac{1 - e^{-2r'l}}{2r'} - \frac{k'^2_\beta r'}{s'} \cdot \frac{1 - e^{-2s'l}}{2s'} - \left(b' - \frac{b'r'}{s'}\right) \frac{1 - e^{-(r'+s')l}}{r' + s'} \right]$$

$$K = \frac{1}{\beta'_0}\left(r^2 \cdot \frac{1 - e^{-2rl}}{2r} + \frac{4k^4_\gamma r^2}{b^2} \cdot \frac{1 - e^{-2sl}}{2s} - \frac{br}{s} \cdot \frac{1 - e^{-(r+s)l}}{r + s} \right)$$

$$L = -\frac{1}{\beta'_0}\cdot 2\cos(k'_\gamma d - k_\gamma d) \cdot\left[(k'_\gamma k_\gamma + r'r)\cdot\frac{1-e^{-(r+r')l}}{r+r'} + \left(\frac{4k'_\gamma k s' s r' r}{bb'} + \frac{4k'^2_\gamma k^2_\gamma r' r}{bb'}\right)\cdot\frac{1-e^{-(s+s')l}}{s+s'}\right] + \frac{1}{\beta'_0}\cdot 2\cos(k'_\gamma d - k_\gamma d) * \left[\left(\frac{2srk'_\gamma k_\gamma}{b} + \frac{2k^2_\gamma r' r}{b}\right)\cdot\frac{1-e^{-(r'+s)l}}{r'+s} + \left(\frac{2s'r'k'_\gamma k_\gamma}{b'} + \frac{2k'^2_\gamma r' r}{b'}\right)\cdot\frac{1-e^{-(r+s')l}}{r+s'}\right]$$

where $A_1 \sim A_5$ and $B_1 \sim B_5$ are constants, μ is the Lame constant of the elastic medium one, d is the in- filled trench width, and l is in- filled trench depth; $r^2(r'^2)$, $s^2(s'^2)$, $a^2(a'^2)$ and $b^2(b'^2)$ can be respectively calculated as

$$\begin{cases} r^2(r'^2) = k^2_\gamma(k'^2_\gamma) - k^2_\alpha(k'^2_\alpha) \\ s^2(s'^2) = k^2_\gamma(k'^2_\gamma) - k^2_\beta(k'^2_\beta) \\ a^2(a'^2) = 2r^2(r'^2) + k^2_\beta(k'^2_\beta) \\ b^2(b'^2) = 2s^2(s'^2) + k^2_\beta(k'^2_\beta) \end{cases} \tag{15}$$

where the parameters with superscript symbol " ' " represent the parameters of medium two, which have the same meaning as the parameters in medium one. α_0' and β_0' can be calculated as

$$\begin{cases} \alpha'_0 = \left(a'^2 + \frac{b'^2 r'}{s'}\right)\cdot\frac{1-e^{-2r'l}}{2r'} + \left(b'^2 + \frac{b'^2 r'}{s'}\right)\cdot\frac{1-e^{-2s'l}}{2s'} - \left(2a'b' + \frac{2b'^2 r'}{s'}\right) \cdot\frac{1-e^{-(r'+s')l}}{r'+s'} \\ \beta'_0 = (k'^2_\gamma + r'^2)\cdot\frac{1-e^{-2r'l}}{2r'} + \frac{b' r'}{s'}\cdot\frac{1-e^{-2s'l}}{2s'} - \frac{b'(s'+r')}{s'}\cdot\frac{1-e^{-(r'+s')l}}{r'+s'} \end{cases} \tag{16}$$

To minimize I_0, $\partial I_0/\partial R' = \partial I_0/\partial T' = 0$:

$$\begin{cases} 2(A+J)(1+R') - 2(B+G)(1-R') + (F+I)T' = 0 \\ 2(C+E+H+K)T' + (D+L) + (F+I)R' = 0 \end{cases} \tag{17}$$

to obtain

$$R' = \frac{X-U}{V-Y},\ T' = X + YR' \tag{18}$$

Among these equations:

$$\begin{cases} X = \frac{-(D+L)}{2(C+E+H+K)} \\ Y = \frac{-(F+I)}{2(C+E+H+K)} \\ U = \frac{2(A+J-B-G)}{-F-I} \\ V = \frac{2(A+J+B+G)}{-F-I} \end{cases} \tag{19}$$

3.3. Rayleigh wave reflection and transmission analysis at the interface of x = 0

As shown in Fig. 3., at the interface (x = 0) between the in-filled trench and the soil, there not only have the incident wave I_1 and the reflected wave I_2 but also have the right-line transmission wave I_3 and the left-line transmission wave I_4.

There have wave amplitude attenuation during wave propagation. The amplitude attenuation of Rayleigh waves only considers geometric attenuation because the dielectric materials are assumed to be a fully elastic body.

When the right-line transmission wave I_3 (the coordinate of x = 0, the amplitude of the wave is A_3) reaches the right side of the in-filled trenches (the coordinate of x = d, the amplitude of wave is A_3'). The distance of d is increased on the propagation path of the waves. The ratio of the amplitude of the two kind waves can be expressed as $\frac{A'_3(x=d)}{A_3(x=0)} = \sqrt{\frac{L_p}{L_p+d}}$, suppose $\beta_{attenuation} = \sqrt{\frac{L_p}{L_p+d}}$.

then there have

$$A'_3|_{x=d} = \beta_{attenuation}\cdot A_3|_{x=0} \tag{20}$$

When the left-wave reflected wave I_4 (the coordinate of x = d, the amplitude of the wave is A_4) reaches the left side of the in-filled trenches (the coordinate of x = 0, the amplitude of the wave is A_4'), due to the secondary reflection, the distance of d is added to the propagation path of the wave. The ratio of the amplitude of the two kind waves can also be expressed as $\frac{A'_4(x=0)}{A_4(x=d)} = \sqrt{\frac{L_p+d}{L_p+2d}}$, suppose $\beta'_{attenuation} = \sqrt{\frac{L_p+d}{L_p+2d}}$.

then there have

$$A'_4|x=0 = \beta'_{attenuation}\cdot A_4|x=0 \tag{21}$$

According to formula 20 and formula 21, we can get the equation $A_4'|_{x=0} = \beta_{attenuation}\cdot\beta'_{attenuation}\cdot R'A_3|_{x=0}$.

At the interface of x = 0, the reflection coefficient R (R = A_2/A_1) and the transmission coefficient T(T = A_3/A_1) can be obtained similar as the calculation process of Equation (12) to Equation (19).

$$R = \frac{X-U}{V-Y},\ T = X + YR \tag{22}$$

Among them,

$$\begin{cases} X = \frac{-(D'+L'+F'+I')}{2(C'+E'+H'+K')} \\ Y = \frac{(-D'-L'+F'+I')}{2(C'+E'+H'+K')} \\ U = \frac{2(A'+J'-B'-G')}{(F'+I'-D'-L')} \\ V = \frac{2(A'+J'+B'+G')}{(F'+I'-D'-L')} \end{cases} \tag{23}$$

the constants A', B',.., I', J', K', L' can be obtained with the following expression:

$$A' = \frac{1}{\alpha_0}\left[a^2\cdot\frac{1-e^{-2rl}}{2r} + b^2\cdot\frac{1-e^{-2sl}}{2s} - 2ab\cdot\frac{1-e^{-(r+s)l}}{r+s}\right] \tag{24}$$

$$B' = \frac{1}{\alpha_0}\cdot\frac{b^2 r}{s}\cdot\left(\frac{1-e^{-2rl}}{2r} + \frac{1-e^{-2sl}}{2s} - 2\cdot\frac{1-e^{-(r+s)l}}{r+s}\right)$$

$$C' = \frac{1}{\alpha_0}\cdot(1+\beta_{attenuation}\beta'_{attenuation}R')^2\left(\frac{\mu'}{\mu}\right)^2\cdot \left(a'^2\cdot\frac{1-e^{-2r'l}}{2r'} + b'^2\cdot\frac{1-e^{-2s'l}}{2s'} - 2a'b'\cdot\frac{1-e^{-(r'+s')l}}{r'+s'}\right)$$

$$D' = -\frac{2}{\alpha_0}(1+\beta_{attenuation}\beta'_{attenuation}R')\left(\frac{\mu'}{\mu}\right) \cdot\left[a'a\cdot\frac{1-e^{-(r+r')l}}{r+r'} + bb'\cdot\frac{1-e^{-(s+s')l}}{s+s'} - ab'\cdot\frac{1-e^{-(r+s')l}}{r+s'} - a'b \cdot\frac{1-e^{-(r'+s)l}}{r'+s}\right]$$

$$E' = \frac{1}{\alpha_0}(1-\beta_{attenuation}\beta'_{attenuation}R')^2\cdot\left(\frac{\mu'}{\mu}\right)^2\cdot\frac{b'^2 r'}{s'} \cdot\left(\frac{1-e^{-2r'l}}{2r'} + \frac{1-e^{-2s'l}}{2s'} - 2\cdot\frac{1-e^{-(r'+s')l}}{r'+s'}\right)$$

$$F' = \frac{-8}{\alpha_0}(1-\beta_{attenuation}\beta'_{attenuation}R')\cdot\left(\frac{\mu'}{\mu}\right)\cdot k'_\gamma k_\gamma r' r.\left(\frac{1-e^{-(r+r')l}}{r+r'}+\frac{1-e^{-(s+s')l}}{s+s'}-\frac{1-e^{-(r+s')l}}{r+s'}-\frac{1-e^{-(r'+s)l}}{r'+s}\right)$$

$$G' = \frac{k_\gamma^2}{\beta_0}\left[\frac{1-e^{-2rl}}{2r}+\frac{4s^2r^2}{b^2}\cdot\frac{1-e^{-2sl}}{2s}-\frac{4sr}{b}\cdot\frac{1-e^{-(r+s)l}}{r+s}\right]$$

$$H' = \frac{k'^2_\gamma}{\beta_0}(1-\beta_{attenuation}\beta'_{attenuation}R')^2\cdot\left(\frac{1-e^{-2r'l}}{2r'}+\frac{4s'^2r'^2}{b'^2}\cdot\frac{1-e^{-2s'l}}{2s'}-\frac{4s'r'}{b'}\cdot\frac{1-e^{-(r'+s')l}}{r'+s'}\right)$$

$$I' = \frac{-2k_\gamma k'_\gamma}{\beta_0}(1-\beta_{attenuation}\beta'_{attenuation}R')\cdot\left(\frac{1-e^{-(r+r')l}}{r+r'}+\frac{4s'sr'r}{bb'}\cdot\frac{1-e^{-(s+s')l}}{s+s'}-\frac{2sr}{b}\cdot\frac{1-e^{-(r'+s)l}}{r'+s}-\frac{2s'r'}{b'}\frac{1-e^{-(r+s')l}}{r+s'}\right)$$

$$J' = \frac{r^2}{\beta_0}\left[\frac{1-e^{-2rl}}{2r}+\frac{4k_\gamma^4}{b^2}\cdot\frac{1-e^{-2sl}}{2s}-\frac{4k_\gamma^2}{b}\frac{1-e^{-(r+s)l}}{r+s}\right]$$

$$K' = \frac{r'^2}{\beta_0}(1+\beta_{attenuation}\beta'_{attenuation}R')^2\cdot\left(\frac{1-e^{-2r'l}}{2r'}+\frac{4k'^4_\gamma}{b'^2}\cdot\frac{1-e^{-2s'l}}{2s'}-\frac{4k'^2_\gamma}{b'}\cdot\frac{1-e^{-(r'+s')l}}{r'+s'}\right)$$

$$L' = -\frac{2rr'}{\beta_0}(1+\beta_{attenuation}\beta'_{attenuation}R').\left[\frac{1-e^{-(r+r')l}}{r+r'}+\frac{4k'^2_\gamma k_\gamma^2}{bb'}\cdot\frac{1-e^{-(s+s')l}}{s+s'}-\frac{2k_\gamma^2}{b}\cdot\frac{1-e^{-(r'+s)l}}{r'+s}-\frac{2k'^2_\gamma}{b'}\cdot\frac{1-e^{-(r+s')l}}{r+s'}\right]$$

Finally, we can obtain the relationship between the incident wave, the transmitted wave and the reflected wave on both sides of the in-filled trenches. When A_1, R, T, R', T' are known, we can obtain the following:

$$\begin{cases} A_2(x=0) = R\cdot A_1(x=0) \\ A_3(x=0) = T\cdot A_1(x=0) \\ A_4(x=0) = \beta'_{attenuation}\cdot A_4(x=d) = \beta'_{attenuation}\cdot R'\beta_{attenuation}\cdot T\cdot A_1(x=0) \\ A_3(x=d) = \beta_{attenuation}\cdot A_3(x=0) = \beta_{attenuation}\cdot T\cdot A_1(x=0) \\ A_4(x=d) = R'A_3(x=d) = R'\beta_{attenuation}\cdot T\cdot A_1(x=0) \\ A_5(x=d) = T'A_3(x=d) = T'\beta_{attenuation}\cdot T\cdot A_1(x=0) \end{cases} \tag{25}$$

According to the relationship between A_i and B_i in Formula 8, respectively, B_i can be calculated sequentially, and the amplitudes of the Rayleigh waves in the entire wave field can be obtained. Furthermore, the function expressions of the reflected Rayleigh waves and transmitted Rayleigh waves near the in-filled trenches can be obtained.

4. Displacements of Rayleigh waves along in-filled trenches

4.1. Displacements under a single-frequency excitation of in-filled trenches

Under the action of a single frequency excitation $f(t) = Pe^{i\omega t}$, the amplitudes $A_1|_{x=0}$ of the incident Rayleigh waves I_1 at the x = 0 position can be expressed as

$$A_{1(x=0)} = \frac{P}{\mu}\chi\sqrt{\frac{1}{L_p\lambda_\gamma}}\cdot\frac{b}{k_\gamma(b-2sr)} \tag{26}$$

To embody the influence of distance attenuation and phase differences, the incident Rayleigh waves I_1 can be expressed with wave potential functions φ_1 and ψ_1.

$$\begin{cases} \varphi_1 = A_1 e^{-rz}e^{i\left(\omega t+\theta-k_\gamma x-k_\gamma L_p-\frac{\pi}{4}\right)} \\ \psi_1 = B_1 e^{-sz}e^{i\left(\omega t+\theta-k_\gamma x-k_\gamma L_p-\frac{\pi}{4}\right)} \end{cases} \tag{27}$$

4.1.1. Displacements in the areas of $x \le 0$

After adding in-filled trenches, the displacements in the area of $x \le 0$ needs to be considered by the superposition effect of the incident wave I_1 and the reflected wave I_2. When the coordinate is $x|_{z=0}$, the horizontal displacement u_x of pickup point can be calculated as

$$u_x = [-k_\gamma A_1\sin(\omega t - k_\gamma x) + k_\gamma A_2\sin(\omega t + k_\gamma x)]\cdot\left(\frac{2sr}{b}-1\right) \tag{28}$$

where A_1 and A_2 are the functions of position x. According to the attenuation laws of Rayleigh waves in an elastic medium, at the position of x = c, we can obtain the following:

$$A_{1(x=c)} = \sqrt{\frac{L_P}{L_P+c}}A_{1(x=0)}$$

$$A_{2(x=c)} = \sqrt{\frac{L_P}{L_P-c}}A_{2(x=0)} \tag{29}$$

According to Formula 25, $A_{2(x=0)} = RA_{1(x=0)}$. By substituting Formula 25, Formula 26 and Formula 27 into Formula 28, the horizontal displacement u_x at the position $x|_{z=0}$ caused by a single-point and single-frequency load can be expressed as

$$u_x = \frac{P}{\mu}\cdot\chi\cdot\sqrt{\frac{1}{L_P\cdot\lambda_\gamma}}\cdot\left[\sqrt{\frac{L_P}{L_P+x}}\sin\left(\omega t+\theta-k_\gamma x-k_\gamma L_p-\frac{\pi}{4}\right)-R\sqrt{\frac{L_P}{L_P-x}}\sin\left(\omega t+\theta+k_\gamma x-k_\gamma L_p-\frac{\pi}{4}\right)\right] \tag{30}$$

Similarly, the vertical displacement w_x at the position $x|_{z=0}$ of pickup point can also be expressed as

$$w_x = \frac{P}{\mu}\cdot\chi\cdot\sqrt{\frac{1}{L_P\cdot\lambda_\gamma}}\cdot\frac{b}{2sk_\gamma}\cdot\left[\sqrt{\frac{L_P}{L_P+x}}\cos\left(\omega t+\theta-k_\gamma x-k_\gamma L_p-\frac{\pi}{4}\right)+R\sqrt{\frac{L_P}{L_P-x}}\cos\left(\omega t+\theta+k_\gamma x-k_\gamma L_p-\frac{\pi}{4}\right)\right] \tag{31}$$

4.1.2. Displacements in the areas of $0 \le x \le d$

Inside in-filled trenches, displacements are generated by superimposing the right-line transmitted wave I_3 and the left-row reflected wave I_4, so the horizontal displacement u_x at the coordinate $x|_{z=0}$ caused by a single-point and single-frequency load can be expressed as

$$u_x = [-k'_\gamma A_3\sin(\omega t - k'_\gamma x) + k'_\gamma A_4\sin(\omega t + k'_\gamma x)]\cdot\left(\frac{2s'r'}{b'}-1\right) \tag{32}$$

The amplitude values A_3 and A_4 are also the functions of x. Considering an in-filled trench medium, Rayleigh wave propagation in the trench medium also conforms to geometric attenuation laws, and it can be obtained as

$$A_{3(x=X)} = \sqrt{\frac{L_P}{L_P + X}} A_{3(x=0)} = \sqrt{\frac{L_P}{L_P + X}} \cdot T \cdot A_{1(x=0)} = \sqrt{\frac{L_P}{L_P + X}} \cdot T \cdot \frac{P}{\mu} \cdot \chi \sqrt{\frac{1}{L_p \lambda_\gamma}} \cdot \frac{b}{k_\gamma (b - 2sr)}$$

$$A_{4(x=X)} = \sqrt{\frac{L_P + d}{L_P + 2d - X}} A_{4(x=d)} = \sqrt{\frac{L_P + d}{L_P + 2d - X}} \cdot R' \cdot A_{3(x=d)} = \sqrt{\frac{L_P}{L_P + 2d - X}} \cdot R' \cdot T \cdot \frac{P}{\mu} \cdot \chi \sqrt{\frac{1}{L_p \lambda_\gamma}} \cdot \frac{b}{k_\gamma (b - 2sr)} \tag{33}$$

Formula 33 is integrated into Formula 32. Considering the phase difference between the incident wave I_3 and the vibration source, the horizontal displacement u_x at the coordinate $x|_{z=0}$ caused by a single-point and single-frequency load can be expressed as

$$u_x = \frac{P}{\mu} \cdot \chi \cdot \sqrt{\frac{1}{L_P \cdot \lambda_\gamma}} \cdot \frac{k'_\gamma \cdot (b' - 2s'r') \cdot b}{k_\gamma \cdot (b - 2sr) \cdot b'} \cdot T \cdot \left[\sqrt{\frac{L_P}{L_P + x}} \sin\left(\omega t + \theta - k'_\gamma x - k_\gamma L_p - \frac{\pi}{4}\right) - R' \sqrt{\frac{L_P}{L_P + 2d - x}} \sin\left(\omega t + \theta + k'_\gamma x - k_\gamma L_p - \frac{\pi}{4}\right) \right] \tag{34}$$

Similarly, the vertical displacement w_x at the position $x|_{z=0}$ of pickup point can also be calculated as

$$w_x = \frac{P}{\mu} \cdot \chi \cdot \sqrt{\frac{1}{L_P \cdot \lambda_\gamma}} \cdot \frac{(b' - 2s'r') \cdot b}{2s' k_\gamma \cdot (b - 2sr)} \cdot T \cdot \left[\sqrt{\frac{L_P}{L_P + x}} \cos\left(\omega t + \theta - k'_\gamma x - k_\gamma L_p - \frac{\pi}{4}\right) + R' \sqrt{\frac{L_P}{L_P + 2d - x}} \cos\left(\omega t + \theta + k'_\gamma x - k_\gamma L_p - \frac{\pi}{4}\right) \right] \tag{35}$$

4.1.3. Displacements in the areas of $x \geq d$

On the right side of the in-filled trenches, under a single-point and single-frequency excitation load, the displacements are determined by transmitted Rayleigh waves I_5. The horizontal displacement u_x at the coordinate $x|_{z=0}$ can be calculated as

$$u_x = k_\gamma \cdot \left(\frac{b - 2sr}{b}\right) \cdot A_5 \cdot \sin(\omega t - k_\gamma x) \tag{36}$$

Attenuation of the Rayleigh wave in the soil conforms to the geometric attenuation laws, obtaining the following:

$$A_{5(x=X)} = \sqrt{\frac{L_P + d}{L_P + X}} A_{5(x=d)} = \sqrt{\frac{L_P + d}{L_P + X}} \cdot T' \cdot A_{3(x=d)} = \sqrt{\frac{L_P}{L_P + X}} \cdot T \cdot T' \cdot \frac{P}{\mu} \cdot \chi \sqrt{\frac{1}{L_p \lambda_\gamma}} \cdot \frac{b}{k_\gamma (b - 2sr)} \tag{37}$$

Formula 37 is integrated into Formula 36. Considering the phase difference between the incident wave I_1 and the vibration source, the horizontal displacement u_x at the coordinate $x|_{z=0}$ caused by a single-point and single-frequency load can be expressed as

$$u_x = \frac{P}{\mu} \cdot \chi \cdot \sqrt{\frac{1}{(L_P + x)\lambda_\gamma}} \cdot TT' \cdot \sin\left(\omega t + \theta - k_\gamma x - k_\gamma L_p - \frac{\pi}{4}\right) \tag{38}$$

Similarly, the vertical displacement w_x at the position $x|_{z=0}$ of the pickup point can also be calculated as

$$w_x = \frac{P}{\mu} \cdot \chi \cdot \sqrt{\frac{1}{(L_P + x) \cdot \lambda_\gamma}} \cdot \frac{b}{2sk_\gamma} \cdot T'T \cdot \cos\left(\omega t - k_\gamma x - k_\gamma L_p - \frac{\pi}{4}\right) \tag{39}$$

4.2. Displacements under a multi-point and multi-frequency excitations of in-filled trenches

A series of the harmonic loads of different frequencies at the same excitation point and different frequencies harmonic loads at different points can be written as follows, respectively:

$$F(t) = \sum_{j=1}^{n} P_j e^{i\left(w_j t + q_j\right)} \text{ (j= 1,2..n) and } \sum F(t) = \sum_{k=1}^{N} \sum_{j=1}^{n} P_{kj} e^{i(\omega_{kj} t + \theta_{kj})} \text{ (j = 1,2..n;k = 1,2..N)} \tag{40}$$

If the excitation forces are non-periodically, it can be converted into a series of periodic concentrated harmonic loads by the Fast Fourier Transform (FFT). The ground vibration inducing by the multi-point and multi-frequency excitation to can be divided into two steps.

Step 1 The ground vibration caused by the multi-frequency excitation at the same point can be obtained by superimposing the excitation responses of different frequencies;

Step 2 Considering the phase difference caused by the difference distance between the excitation point and the in-filled trenches, the ground vibration responses induced by a series of the multi-point and multi-frequency excitation can be get by superimposing the multi-frequency excitation responses at the same point.

4.2.1. Displacement in the areas of $x \leqq 0$

The surface displacement u_x and w_x under a series of different frequencies harmonic loads at the same point can be calculated as

$$\begin{cases} u_x = \sum_{j=1}^{n} u_j = \sum_{j=1}^{n} \frac{P_j}{\mu} \cdot \chi \cdot \left[\sqrt{\frac{1}{(L_p + x)\lambda_{\gamma j}}} \cdot \sin(\omega_j t + \theta_j - k_{\gamma j} x - k_{\gamma j} L_p - \pi/4) - R_j \sqrt{\frac{1}{(L_p - x)\lambda_{\gamma j}}} \cdot \sin(\omega_j t + \theta_j + k_{\gamma j} x - k_{\gamma j} L_p - \pi/4) \right] \\ w_x = \sum_{j=1}^{n} w_j = \sum_{j=1}^{n} \frac{P_j}{\mu} \chi \cdot \frac{b}{2k_\gamma s} \cdot \left[\sqrt{\frac{1}{(L_p + x)\lambda_{\gamma j}}} \cdot \cos(\omega_j t + \theta_j - k_{\gamma j} x - k_{\gamma j} L_p - \pi/4) + R_j \sqrt{\frac{1}{(L_p - x)\lambda_{\gamma j}}} \cdot \cos(\omega_j t + \theta_j + k_{\gamma j} x - k_{\gamma j} L_p - \pi/4) \right] \end{cases} \tag{41}$$

Considering a series of different frequencies harmonic loads at the different points, the surface displacements u_x and w_x can be calculated as.

$$\begin{cases} u_x = \sum_{k=1}^{N} \sum_{j=1}^{n} \frac{P_{kj}}{\mu} \chi \cdot \left[\sqrt{\frac{1}{(L_{pk} + x)\lambda_{\gamma kj}}} \cdot \sin(\omega_{kj} t + \theta_{kj} - k_{\gamma kj} x - k_{\gamma kj} L_{pk} - \pi/4) - R_{kj} \cdot \sqrt{\frac{1}{(L_{pk} - x)\lambda_{\gamma kj}}} \sin(\omega_{kj} t + \theta_{kj} + k_{\gamma kj} x - k_{\gamma kj} L_{pk} - \pi/4) \right] \\ w_x = \sum_{k=1}^{N} \sum_{j=1}^{n} \frac{P_{kj}}{\mu} \chi \cdot \frac{b}{2k_\gamma s} \cdot \left[\sqrt{\frac{1}{(L_{pk} + x)\lambda_{\gamma kj}}} \cdot \cos(\omega_{kj} t + \theta_{kj} - k_{\gamma kj} x - k_{\gamma kj} L_{pk} - \pi/4) + R_{kj} \cdot \sqrt{\frac{1}{(L_{pk} - x)\lambda_{\gamma kj}}} \cos(\omega_{kj} t + \theta_{kj} + k_{\gamma kj} x - k_{\gamma kj} L_{pk} - \pi/4) \right] \end{cases} \tag{42}$$

4.2.2. Displacement in the areas of $0 \leq x \leq d$

The surface displacement u_x and w_x under a series of different frequencies harmonic loads at the same point can be expressed as

$$\begin{cases} u_x = \sum_{j=1}^{n} u_j = \sum_{j=1}^{n} \frac{P_j}{\mu}\cdot\chi\cdot\frac{k'_\gamma\,(b'-2s'r')b}{k_\gamma(b-2sr)b'}\cdot T_j\cdot \\ \quad \left[\sqrt{\frac{1}{(L_p+x)\lambda_{\gamma j}}}\cdot\sin(\omega_j t+\theta_j-k'_{\gamma j}x-k_{\gamma j}L_p-\pi/4)-R'_j\right. \\ \quad \left.\sqrt{\frac{1}{(L_p+2d-x)\lambda_{\gamma j}}}\cdot\sin(\omega_j t+\theta_j+k'_{\gamma j}x-k_{\gamma j}L_p-\pi/4)\right] \\ w_x = \sum_{j=1}^{n} w_j = \sum_{j=1}^{n} \frac{P_j}{\mu}\chi\cdot\frac{(b'-2s'r')b}{2k_\gamma s'(b-2sr)}\cdot T_j\cdot \\ \quad \left[\sqrt{\frac{1}{(L_p+x)\lambda_{\gamma j}}}\cdot\cos(\omega_j t+\theta_j-k'_{\gamma j}x-k_{\gamma j}L_p-\pi/4)\right. \\ \quad \left.+R'_j\sqrt{\frac{1}{(L_p+2d-x)\lambda_{\gamma j}}}\cdot\cos(\omega_j t+\theta_j+k'_{\gamma j}x-k_{\gamma j}L_p-\pi/4)\right] \end{cases} \tag{43}$$

Considering a series of different frequencies harmonic loads at the different points, the surface displacement u_x and w_x can be calculated as

$$\begin{cases} u_x = \sum_{k=1}^{N}\sum_{j=1}^{n} \frac{P_{kj}}{\mu}\cdot\chi\cdot\frac{k'_\gamma\,(b'-2s'r')b}{k_\gamma(b-2sr)b'}\cdot T_{kj}\cdot\left[\sqrt{\frac{1}{(L_{pk}+x)\lambda_{\gamma kj}}}\cdot\sin(\omega_{kj}\right. \\ \quad t+\theta_{kj}-k'_{\gamma kj}x-k_{\gamma kj}L_{pk}-\pi/4)-R'_{kj}\sqrt{\frac{1}{(L_{pk}+2d-x)\lambda_{\gamma kj}}}\cdot\sin(\omega_{kj} \\ \quad \left.t+\theta_{kj}+k'_{\gamma kj}x-k_{\gamma kj}L_{pk}-\pi/4)\right] \\ w_x = \sum_{k=1}^{N}\sum_{j=1}^{n} \frac{P_{kj}}{\mu}\cdot\chi\cdot\frac{(b'-2s'r')b}{2s'k_\gamma(b-2sr)}\cdot T_{kj}\cdot\left[\sqrt{\frac{1}{(L_{pk}+x)\lambda_{\gamma kj}}}\cdot\cos(\omega_{kj}\right. \\ \quad t+\theta_{kj}-k'_{\gamma kj}x-k_{\gamma kj}L_{pk}-\pi/4)+R'_{kj}\sqrt{\frac{1}{(L_{pk}+2d-x)\lambda_{\gamma kj}}}\cdot\cos(\omega_{kj} \\ \quad \left.t+\theta_{kj}+k'_{\gamma kj}x-k_{\gamma kj}L_{pk}-\pi/4)\right. \end{cases} \tag{44}$$

4.2.3. Displacement in the areas of $x \geq d$

The surface displacement u_x and w_x under a series of different frequencies harmonic loads at the same point can be expressed as

$$\begin{cases} u_x = \sum_{j=1}^{n} u_j = \sum_{j=1}^{n} \frac{P_j}{\mu}\cdot\chi\cdot\sqrt{\frac{1}{(L_p+x)\lambda_{\gamma j}}}\cdot T_j T_j \\ \quad '\cdot\sin\left(\omega_j t+\theta_j-k_{\gamma_j}x-k_{\gamma_j}L_p-\frac{\pi}{4}\right) \\ w_x = \sum_{j=1}^{n} w_j = \sum_{j=1}^{n} \frac{P_j}{\mu}\cdot\chi\cdot\sqrt{\frac{1}{(L_p+x)\lambda_{\gamma j}}}\cdot\frac{b}{2sk}\cdot T_j T_j \\ \quad '\cdot\cos\left(\omega_j t+\theta_j-k_{\gamma_j}x-k_{\gamma_j}L_p-\frac{\pi}{4}\right) \end{cases} \tag{45}$$

Considering a series of different frequencies harmonic loads at the different points, the surface displacement u_x and w_x can be calculated as

$$\begin{cases} u_x = \sum_{k=1}^{N}\sum_{j=1}^{n} \frac{P_{kj}}{\mu}\cdot\chi\cdot T_{kj}\,T'_{kj}\cdot\sqrt{\frac{1}{(L_{pk}+x)\lambda_{\gamma kj}}}\cdot\sin(\omega_{kj}t+\theta_{kj}-k_{\gamma kj}x-k_{\gamma kj} \\ \quad L_{pk}-\pi/4) \\ \quad w_x = \sum_{k=1}^{N}\sum_{j=1}^{n} \frac{P_{kj}}{\mu}\cdot\chi\cdot\frac{b}{2sk}\cdot T_{kj}\,T'_{kj}\cdot\sqrt{\frac{1}{(L_{pk}+x)\lambda_{\gamma kj}}}\cdot\cos(\omega_{kj} \\ \quad\quad t+\theta_{kj}-k_{\gamma kj}x-k_{\gamma kj}L_{pk}-\pi/4) \end{cases} \tag{46}$$

From Formula 40 to Formula 46, where the subscripts k and j represent changes in the position of the excitation point and different frequencies of the excitation force, respectively; u_x and w_x represents the horizontal and vertical displacements of ground surface points, respectively; P_{kj} is the load magnitude at the k-point; L_{pk} is the distance from the k excitation point to the left side of the in-filled trench; R_{kj}, T_{kj}, R'_{kj}, T'_{kj} are the transmission and reflection coefficients at the contact surfaces on both sides of the trench, respectively.

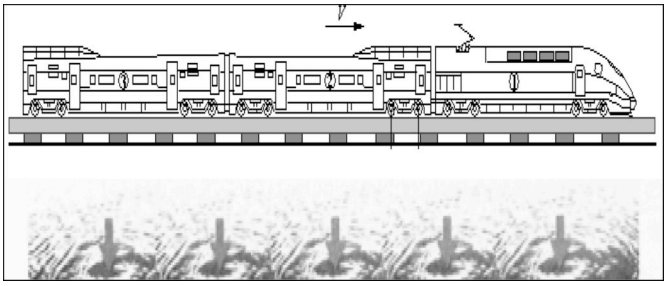

Fig. 4. Decentralized fixed-point vibration excitation induced by a train.

5. The vibration isolation analysis of in-filled trench parameters

Moving excitation will be generated along the track direction when a train is running (Fig. 4). The excitation will produce a non-periodic concentrated vertical dynamic reaction forces on the foundation soil. Under the vertical concentrated force, the vibration wave propagating to the distant places will be generated in the soil. When considering the vibration responses of the far field soil, since the body wave attenuation is faster, only the contribution of the Rayleigh wave field to the vibration can be considered.

The vibration responses induced by a running train can be superimposed by a plurality of concentrated harmonic loads, and the phase changes caused by the time and position factors need to be considered, as shown in Fig. 5, where d is the distance between the front and rear wheels.

The ground vibrations induced by running train are related to many factors. This paper uses the formulas of the previous section to analyse the soil vibration isolation effects with the parameter changes of an in-filled trench, such as trench width, trench depth and changes in the in-filled material.

5.1. Calculation parameters

5.1.1. Excitation force parameters

The Nanjing light rail passenger train is selected as a sample for calculations, and the train speed is considered as 60 km/h. The spectrum curves and time history curves of the orbital dynamic reaction are as shown in Fig. 6. Due to attenuation faster of the high frequency vibration, only the spectrum analysis of the part below 40 Hz is intercepted. The midpoint of the excitation point of each train is o point, and the excitation points quantity is 13 (N = 13). The spacing between each excitation point is 3 m (lc = 3 m), and the distance between the excitation centre point, and the left side of the trenches is Lp = 25 m.

5.1.2. Other parameters

The soil is selected from the typical medium soft soil, for which Poisson's ratio is $\xi = 0.3$, the elastic modulus is $E = 270 \times 10^6$pa, and the mass density is $\rho = 1800\,kg/m^3$.

The in-filled material properties of trenches have a great influence on the vibration isolation. According to the characteristic differences between the in-filled materials and the soil. There have four kinds of in-filled trench materials are selected by depending on the different elastic

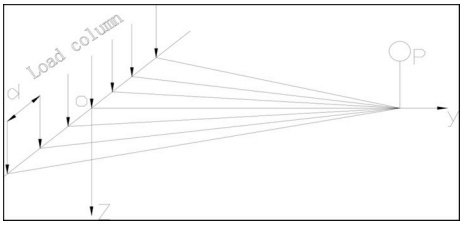

Fig. 5. Superimposed multiple vertical harmonic loads.

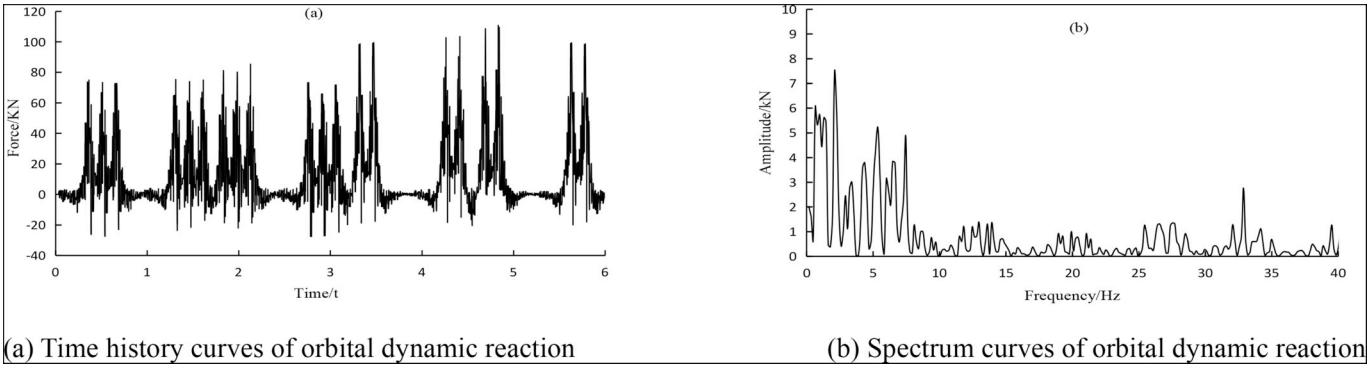

Fig. 6. Time history curves and spectrum curves of orbital dynamic reaction under running train.

Table 1
The parameter table of in-Filled materials.

In-filled materials	Elastic modulus (pa)	Density (kg/m^3)	Poisson's ratio(ν)	Damping ratio (ξ)
Sand gravel	5×10^8	2100	0.24	0.05
Fly ash	25×10^6	500	0.35	0.1
Concrete	3×10^{10}	2500	0.2	0.05
Foam material	2×10^6	30	0.25	0.12

modulus of in-filled material. The various in-filled material parameters are shown in Table 1.

5.2. Vibration isolation analysis of in-filled trench parameters

5.2.1. Vibration response comparison of pick-up point under the variation of trench width

The trench depth is h = 8 m, and sand gravel is selected as in-filled trench material. Five kinds of working conditions, such as 0, 1, 2, 3, and 4 m, are selected for analysis. The pick-up point is 30 m away from the centre line of the track.

Under the action of running trains, the variations of vertical acceleration level along with the trench widths are shown in Table 2, the variations of reflection amplitude ratio and transmission amplitude ratio along with the trench widths are shown in Fig. 7(a), and the variations of the vertical acceleration spectrum along with the trench widths are shown in Fig. 7 (b).

Table 2 shows that the vertical acceleration level of the pick-up point is gradually decreases with the increase of trench widths, and the vibration isolation effect is more obvious.

Fig. 7(a) shows that the amplitude ratio of the transmitted wave is gradually decreases with the increase of trench widths. When the trench width exceeds a certain limit, the amplitude of the transmitted wave increases as the trench width increases. Therefore, in order to obtain a better vibration isolation effect, the trench width must be strictly controlled.

Fig. 7(b) indicates that the amplitudes of the vertical acceleration spectrum of the pickup point gradually decreases with the increase of trench widths, and the high frequencies decrease more than the low frequencies. The variations of trench widths do not affect the distribution of the main frequency band in the acceleration spectrum.

Table 2
The vertical acceleration levels of soil surface point varies with trench widths (dB).

Vibration level	d = 1 m	d = 2 m	d = 3 m	d = 4 m
V60	69.21	68.45	66.77	65.74

5.2.2. Comparison of vibration responses of pick-up point under the variation of trench depths

The trench width is d = 2 m, and the sand gravel is selected as in-filled trench material. The analysis of trench depth h selects 5 kinds of working conditions such as 0, 2, 4, 6, and 8 m. The pick-up point is 28 m away from the centre line of the track.

Under the action of running trains, the variations of the vertical acceleration level and the trench depths are shown in Table 3, the variations of reflection amplitude ratio and transmission amplitude ratio along with the trench depths are shown in Fig. 8 (a). The variations of the vertical acceleration spectrum along with the trench depths are shown in Fig. 8 (b).

Fig. 8(a) shows that variations of trench depths have little effect on the transmission coefficient of Rayleigh waves. As the trench depth increases, the transmission amplitude ratios remain relatively unchanged.

Table 3 and Fig. 8(b) show that the acceleration levels and spectrum peaks of the pick-up point are also only slightly reduced with increasing trench depth. The vibration isolation influence of trench depths change is not obvious, but in order to reduce the influence of Rayleigh waves diffraction at the trench bottom, the critical depth of the in-filled trench should be set to one Rayleigh wave wavelength [28].

5.2.3. Comparison of vibration responses under the material characteristic variation of in-filled trenches

The trench width d and depth h are selected as 2 m and 8 m, respectively. The pick-up point is 28 m away from the centre line of the track. Under the action of running trains, the variations of the vertical acceleration level along with the difference of in-filled materials are shown in Table 4, the variations of reflection amplitude ratio and transmission amplitude ratio along with the difference of in-filled materials are shown in Fig. 9 (a), and the variations of the vertical acceleration spectrum along with the difference of in-filled materials are shown in Fig. 9 (b).

Fig. 9(a) shows the wave transmittance increases with the increase of trench medium density, when the density of trench medium is close to the density of soil, the transmittance reaches the maximum. After the soil density is exceeded, the wave transmittance is smaller with the increasing in-filled mediums density.

Table 4 and Fig. 9(b) show that the greater difference between the in-filled trench materials and the soil, the better the vibration isolation effect. The vibration isolation effect of the foam board is the best, and the vibration isolation effect of the gravel soil is the worst. The amplitudes of the spectrum decrease regularly as the difference in the filled materials increases but does not affect the distribution of the main frequency bands.

6. Theoretical model verification

To verify the theoretical calculations, a finite element model

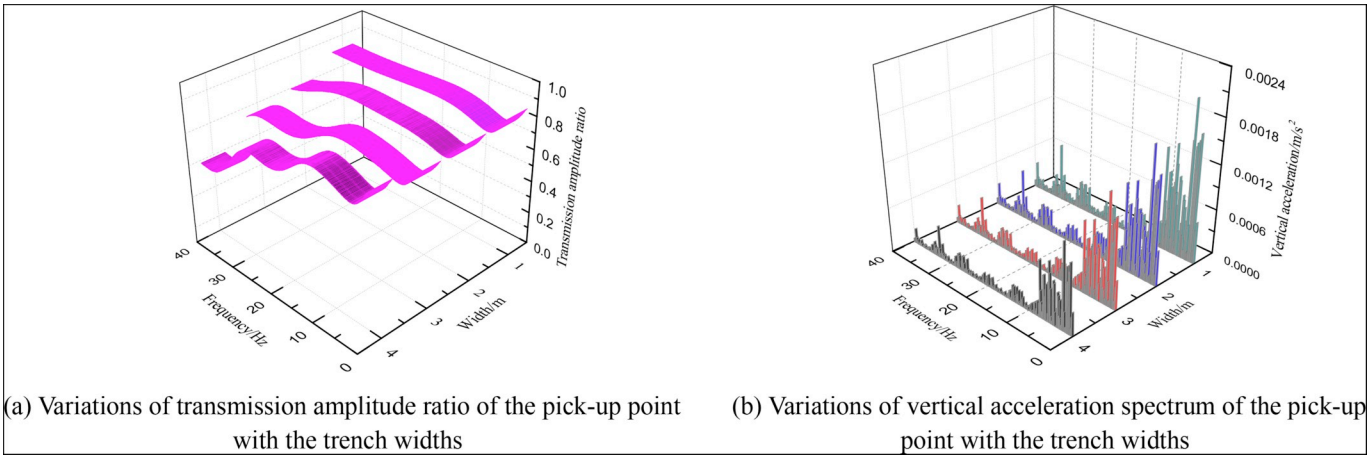

(a) Variations of transmission amplitude ratio of the pick-up point with the trench widths

(b) Variations of vertical acceleration spectrum of the pick-up point with the trench widths

Fig. 7. Variations of transmission amplitude ratio and vertical acceleration spectrum of the pick-up point with the trench widths.

Table 3
The vertical acceleration levels of soil surface points varies with trench depths (dB).

Vibration level	h = 2 m	h = 4 m	h = 6 m	h = 8 m
V60	70.57	69.94	69.38	69.62

Table 4
Vertical acceleration levels of soil surface point varies with in-filled materials (dB).

Vibration level	Sand gravel	Fly ash	Concrete	Foam material
V60	69.62	68.35	66.57	62.05

containing a train-soil-trench system was established.

6.1. Train-ground-trench FE model

6.1.1. Train-track system model

The train-track system model consists of a vehicle model and a track model connected by the assumed wheel-track relation. The system model can be shown in Fig. 10, which can be seen a previous study [23]. Vibrations in the vertical direction are more significant than those in other directions, so only the vertical vibration is considered in this model.

5.1.1.1. Vehicle model. The vehicle model is composed of many carriages in a train. Each carriage is a multiple-degree-of-freedom vibration system composed by one car, two bogies, four wheels, and two groups of spring-damper suspension systems. Two degrees-of-freedom (Z) and (RX) are considered for each car or bogie. Only one degree-of-freedom (Z) is considered for each wheel. The vehicle motion equation is established based on the La- grange motion equation, which is described as follows:

$$\frac{d}{dt}\left(\frac{\partial T}{\partial \dot{q}_k}\right) - \frac{\partial T}{\partial q_k} + \frac{\partial V}{\partial q_k} + \frac{\partial Q}{\partial \dot{q}_k} = 0 \tag{47}$$

where T, V and Q are the total kinetic energy, total elastic potential energy and total damper dissipation energy of the motion system, respectively.

The motion system of the body, bogie and wheel-set can be established based on the Lagrange motion equation. The motion equation of the ith body and its two bogies is as follows:

$$M_i\ddot{Z}_i + C_i\dot{Z}_i + K_iZ_i = P_i(t),\ i = 1,2,\cdots,N_v \tag{48}$$

where Z_i is the displacement vector of the ith vehicle; $P_{i(t)}$ is the external excitation force for the ith vehicle, and M_i, C_i, K_i show the mass, damping and stiffness of the ith vehicle model, respectively.

5.1.1.2. Track model. The track is simplified to a 3-level mass-spring-damper system, in which the influences of rail, ballast, sleeper and

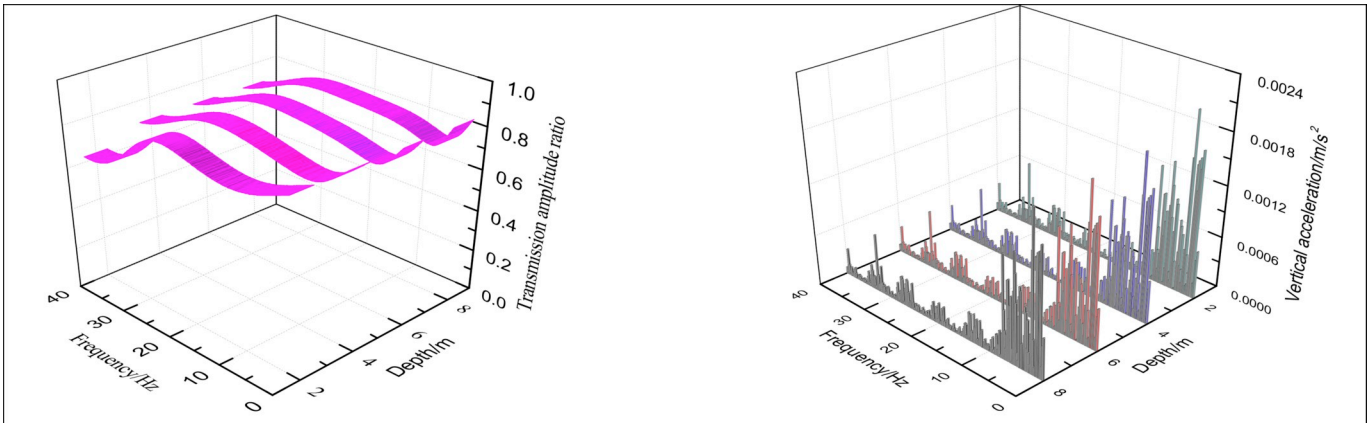

(a) Variations of transmission amplitude ratio of the pick-up point with the trench depths

(b) Variations of vertical acceleration spectrum of the pick-up point with the trench depths

Fig. 8. Variations of transmission amplitude ratio and vertical acceleration spectrum of the pick-up point with the trench depths.

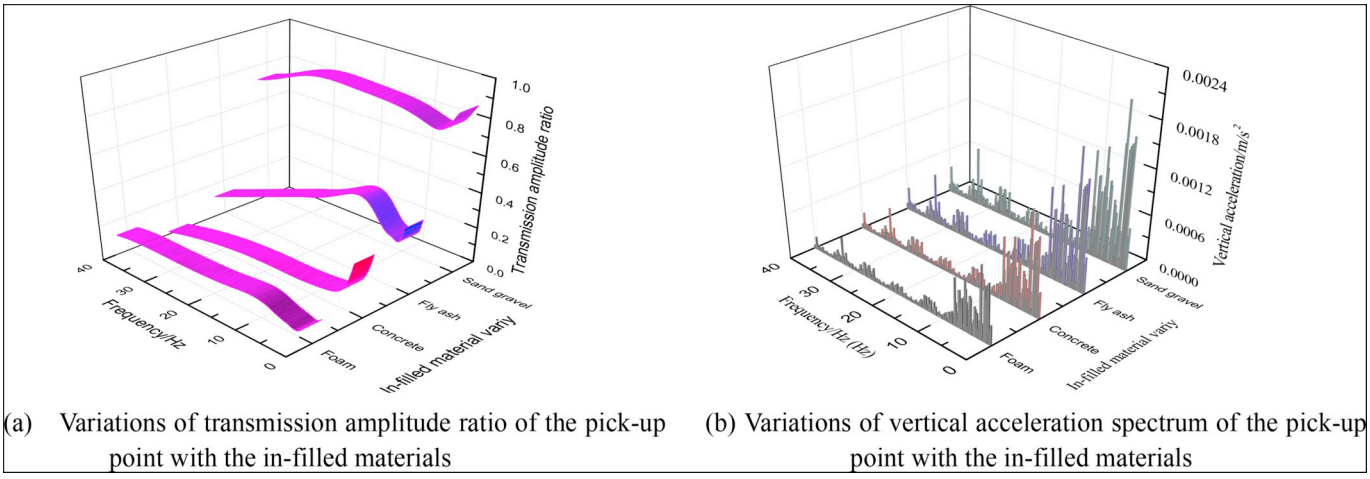

(a) Variations of transmission amplitude ratio of the pick-up point with the in-filled materials

(b) Variations of vertical acceleration spectrum of the pick-up point with the in-filled materials

Fig. 9. Variations of transmission amplitude ratio and vertical acceleration spectrum of the pick-up point with the in-filled materials.

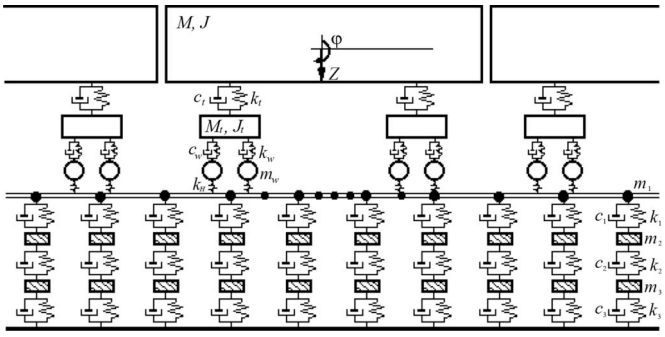

Fig. 10. Train-track system model.

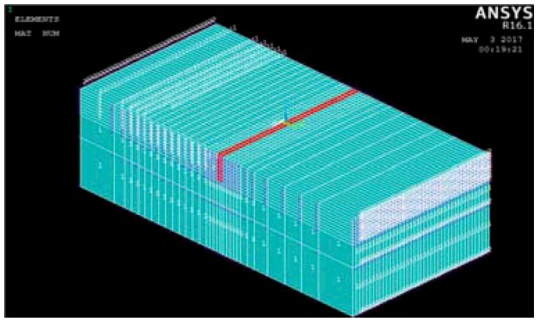

Fig. 11. Soil - infilled trench analysis model.

roadbed are considered. The wheel-set connects with the track in accordance with a Hertz wheel-rail contact relationship. The vibration in the vertical longitudinal plane of the model is only considered. It is due to that the vertical excitation for the bottom roadbed caused by the locomotive axle load of the moving train is much larger than the horizontal excitation.

In Fig. 11, c_1,c_2,c_3,m_1,m_2,m_3,k_1,k_2 and k_3 are the damping, mass and stiffness of a 3-layer mass spring damper for the track system, respectively.

Table 6
Vertical vibration acceleration level varies with trench width.

Trench width (m)	Model calculation results(dB)	Formula calculation results(dB)	Data difference (dB)
0	71.98	70.59	+1.39
1	70.85	69.21	+1.64
2	69.64	68.58	+1.06
3	68.72	66.77	+1.95
4	67.98	65.34	+2.64

Table 7
Vertical vibration acceleration level varies with trench depth.

Trench depth (m)	Model calculation results(dB)	Formula calculation results(dB)	Data difference (dB)
0	71.98	70.59	+1.39
2	71.42	69.86	+1.56
4	70.64	69.32	+1.32
6	70.12	68.94	+1.18
8	69.64	68.58	+1.06

6.1.2. Soil-trench system model

The soil-infilled trench finite element model is shown in Fig. 11. The following describes various assumptions used in the analysis.

The soil is regarded as linear elastic and laminated. In the finite element analysis, the soil model uses a solid45 unit, the relation

Table 5
Different influencing factors and working condition setting.

Influencing factor	Invariant parameters	Train incentive	Working condition setting	Pickup point position
Trench width(d)	Depth (h = 8 m) Distance from source (Lp = 25 m) In-filled trench material (Sand gravel)	Nanjing Light Rail Train (60 km/h)	d = 0 m; d = 1 m; d = 2 m; d = 3 m; d = 4 m	From the vibration source:(28 m)
Trench depth(h)	Width (d = 2 m) Distance from source (Lp = 25 m) In-filled trench material (Sand gravel)	Nanjing Light Rail Train (60 km/h)	h = 0 m; h = 2 m; h = 4 m; h = 6 m; h = 8 m	From the vibration source:(28 m)
In-filled material	Width (d = 2 m) Depth (h = 8 m) Distance from source (Lp = 25 m)	Nanjing Light Rail Train (60 km/h)	Sand grave; Fly ash; Concrete; Foam material	From the vibration source:(28 m)

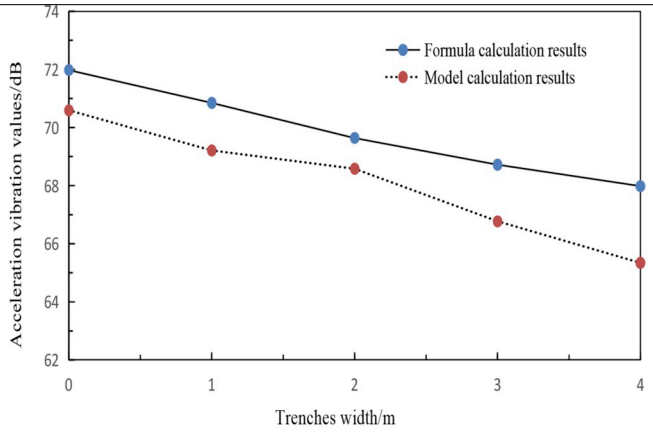

(a) Two calculation curve comparison under the width changes of trenches

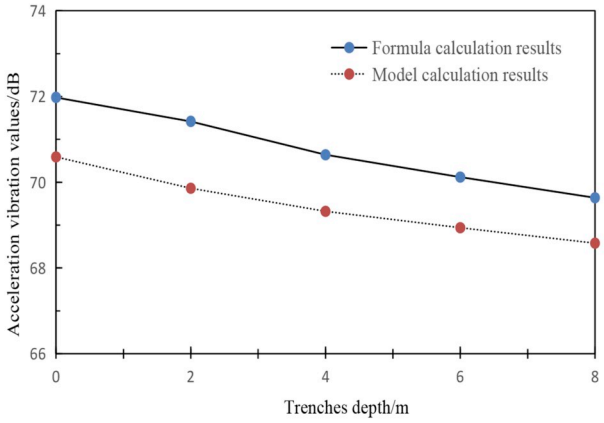

(b) Two calculation curve comparison under depth changes of trenches

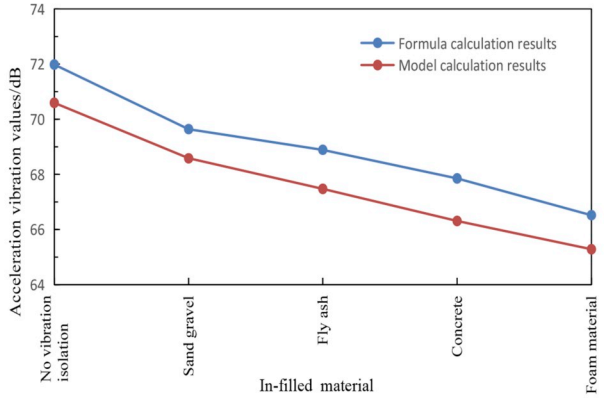

(c) Two calculation curve comparison under in-filled material changes of trenches

Fig. 12. Two calculation curve comparison under the width, depth and in-filled material changes of trenches.

between the surrounding soil and the in-filled trenches is considered as spring contact. The nodes between the soil and the in-filled trenches are treated by a spring, and the spring coefficient k is determined by the reflection coefficient.

The sizes of the model are set as follows: the length of the model is 120 m along the track, the width of the vertical track is 80 m, the depth of model is 20 m, and the size of model unit is select as 3 m (Fig. 11). The artificial boundary of soil side is regarded as a viscous-spring material, and the boundary of bottom surface is consolidation, and the damp coefficient value of spring is ρ_v, and the elastic coefficient value is G/2rb [24,25].

6.1.3. Calculation parameters of model

The parameters of soil are set as follows: Poisson's ratio is 0.33,

Table 8
Vertical vibration acceleration level varies with in-filled materials.

In-filled trench material	Model calculation results(dB)	Formula calculation results(dB)	Data difference(dB)
No vibration isolation	71.98	70.59	+1.67
Sand gravel	69.64	68.58	+2.06
Fly ash	68.89	67.47	+1.39
Concrete	67.85	66.31	+1.54
Foam material	66.52	65.28	+1.24

elastic modulus is $E = 270 \times 10^6$pa, mass density is $\rho = 1800\,kg/m^3$, and shear wave speed is $c_s = 240\,m/s$.

In the calculation, the Nanjing light rail passenger marshaling is set as 1 trailer + 6 motor car +1 trailer, and the train speed is set to v = 60 km/h.

6.1.4. Design of calculation conditions

To compare the calculation results between the finite element model and the formulas, the in-filled trench parameters in the finite element model are consistent with that of the formulas, as shown in Table 5.

6.2. Analysis of calculation results

The calculation result comparison between the numerical analysis and the formulas on the change of the in-filled trench parameter are shown in Table 6 to Table 7, and the curve comparison between the two calculation results is shown in Fig. 12.

From Table 7 to Table 8 and Fig. 12, the following determinations can be made:

(1) The vibration isolation effects become better with the in-filled trench width increasing, and the ground vibrations decrease slowly with the increase of the in-filled trench depth, however, in order to reduce the influence of the Rayleigh wave diffraction at the bottom of the barrier, according to some research results [15,26,27], the minimum depth of trench should be at least $0.6L_R$ at a point $10L_R$ away from such trench for the active isolation and $1.33L_R$ for the passive. In the influence law of the vibration isolation effect, the numerical analysis results are consistent with the formula calculation results.
(2) Because of unconsidered the energy loss of the cross-section between soil and trench in the model, the vertical acceleration vibration values calculated by the numerical model are greater than the corresponding formulas calculation values.

7. Conclusions

According to the propagation characteristics of the Rayleigh waves passing through in-filled trenches, the paper analyses the reflection coefficients and transmission coefficients of Rayleigh waves at the interface between in-filled trenches and the soil. In our calculation formulas of ground vibrations, a single point and a single frequency excitation, as well as multi-points and multi-frequencies excitation, are simultaneously derived in the soil-in-filled-trench system.

From the results of numerical analysis and formulas calculations, the following can be found:

The vibration levels of the pick-up point will be reduced after vibration isolation of in-filled trenches. The vertical acceleration level and amplitude ratio of the transmitted wave all decreased with the in-filled trench width increasing. The more differences of density and elastic modulus between in-filled materials and soil properties, the larger the reflection coefficient, the better vibration isolation effect. The changes of the trench depth have little influence on the transmission coefficient and vibration isolation effects of soil, however, there should be a minimum infilled trench depth in order to reduce the influence of the Rayleigh wave diffraction at the bottom of the barrier.

The calculation results of the formulas are basically consistent with the numerical analysis results, which indicates that the theoretical derivation formulas can be used to analyse the environmental vibration influence of in-filled trenches induced by a running train.

Author Contributions

Jinbao Yao participated in the guidance of the theoretical derivation part of the paper, the establishment, calculation and analysis of numerical models, the writing of papers, etc.

Rutao Zhao participated in the theoretical derivation of the Rayleigh wave reflection and transmission coefficients on the contact surface and the displacement calculation formulas.

Nan Zhang participated in the establishment of the train-track model.

Dujuan Yang participated in the overall framework design, critical revision of this paper and commented on the manuscript.

Acknowledgments

This research is supported in part by the Basic Research Funds of Beijing Jiaotong University (C17JB00440).

Appendix A. Supplementary data

Supplementary data to this article can be found online at https://doi.org/10.1016/j.soildyn.2019.105741.

References

[1] François S, Pyl L, Masoumi HR, Degrande G. The influence of dynamic soil–structure interaction on traffic induced vibrations in buildings. Soil Dynam Earthq Eng 2007;27(7):655–74.
[2] Bajcar T, Cimerman F, Širok B, Ameršek M. Impact assessment of traffic-induced vibration on natural gas transmission pipeline. J Loss Prev Process Ind 2012;25(6):1055–68.
[3] Bian X, Jiang H, Chang C, Hu J, Chen Y. Track and ground vibrations generated by high-speed train running on ballastless railway with excitation of vertical track irregularities. Soil Dynam Earthq Eng 2015;76:29–43.
[4] Leonardi G, Buonsanti M. Reduction of train-induced vibrations by using barriers. Res J Appl Sci Eng Technol 2014;7(17):3623–32.
[5] Yaseri A, Bazyar MH, Javady S. 2.5 D coupled FEM-SBFEM analysis of ground vibrations induced by train movement. Soil Dynam Earthq Eng 2018;104:307–18.
[6] Persson P, Persson K, Sandberg G. Numerical study of reduction in ground vibrations by using barriers. Eng Struct 2016;115:18–27.
[7] Woods RD. Screening of surface waves in soils. J Soil Mech Found Div 1968;94(4):221–314.
[8] Beskos DE, Dasgupta B, Vardoulakis IG. Vibration isolation using open or filled trenches. Comput Mech 1986;1(1):43–63.
[9] Yang YB, Hung HH. A parametric study of wave barriers for reduction of train-induced vibrations. Int J Numer Methods Eng 1997;40(20):3729–47.
[10] Xu HY, Chen DY, Yang XJ, Liang B. Propagation characteristics of plane SH wave passing through elastic interlining in elastic medium. Chin J Rock Mech Eng 2003;2. 030.
[11] Andersen L, Nielsen SR, Krenk S. Numerical methods for analysis of structure and ground vibration from moving loads. Comput Struct 2007;85(1–2):43–58.
[12] Adam M, Von Estorff O. Reduction of train-induced building vibrations by using open and filled trenches. Comput Struct 2005;83(1):11–24.
[13] Celebi E, Kırtel O. Non-linear 2-D FE modeling for prediction of screening performance of thin-walled trench barriers in mitigation of train-induced ground vibrations. Constr Build Mater 2013;42:122–31.
[14] Lysmer J, Waas G. Shear waves in plane infinite structures. J Eng Mech 1972;98(1):85–105.

[15] Ahmad S, Al-Hussaini TM. Simplified design for vibration screening by open and in-filled trenches. J Geotech Eng 1991;117(1):67–88.
[16] Bose T, Choudhury D, Sprengel J, Ziegler M. Efficiency of open and Infill trenches in mitigating ground-Borne vibrations. J Geotech Geoenviron Eng 2018;144(8):04018048.
[17] Zoccali P, Cantisani G, Loprencipe G. Ground-vibrations induced by trains: filled trenches mitigation capacity and length influence. Constr Build Mater 2015;74:1–8.
[18] Garinei A, Risitano G, Scappaticci L. Experimental evaluation of the efficiency of trenches for the mitigation of train-induced vibrations. Transport Res Part D 2014;32:303–15.
[19] Jones CJC. Low frequency ground vibration. In: Thompson DJ, editor. Railway noise and vibration: mechanisms, modelling and means of control. Oxford, UK: Elsevier; 2008. p. 399–433.
[20] De Bremaecker JC. Transmission and reflection of Rayleigh waves at corners. Geophysics 1958;23(2):253–66.
[21] Lapwood ER. The transmission of a Rayleigh pulse round a corner. Geophys J R Astron Soc 1961;4:174–96.
[22] Li Y, Wei PJ, Tang Q. Reflection and transmission of elastic waves at the interface between two gradient-elastic solids with surface energy. Eur J Mech A Solid 2015;52:54–71.
[23] Zhang N, Xia H, Yang WG, Zhao SY. Prediction and control of building vibration under metro excitations. Proceedings of the 8 th international conference on structural dynamics, Leuven. 2011. p. 705–11.
[24] Liu JB, Gu Y, Du YX. Consistent viscous-spring artificial boundaries and viscous-spring boundary elements. Yan Tu Gong Cheng Xue Bao 2006;28(9):1070–5.
[25] Du X, Zhao M. A local time-domain transmitting boundary for simulating cylindrical elastic wave propagation in infinite media. Soil Dynam Earthq Eng 2010;30(10):937–46.
[26] Haupt WA. Model tests on the screening of surface waves. Proceedings of the Tenth International Conference on soil mech. found. eng. Vol. 3. Stockholm. 1981. p. 215–22.
[27] Yao JB, Xia H, Zhang N, Yu B. Prediction on building vibration induced by moving train based on support vector machine and wavelet analysis. J Mech Sci Technol 2014;28(6):2065–74.
[28] Gao GY, Li ZY, Qiu C. Three-dimensional analysis of in-filled trench as barriers for isolating vibration in far field. Rock Soil Mech-Wuhan 2005;26(8):1184–90.